

Final Report

**Finite Element Analysis on
Caverns 33 and 43,
34/44 LPG Gallery, Gallery 10, and Well 58
of Finger Lakes LPG Storage, LLC**

Prepared for

International Gas Consulting
Houston, Texas

By

K. Fuenkajorn, Ph.D., P.E.
Geomechanics Research Unit
Suranaree University of Technology
Thailand

September 2010

TABLE OF CONTENTS

	Page
EXECUTIVE SUMMARY.....	1
1. INTRODUCTION.....	2
2. SITE AND CAVERN CHARACTERISTICS.....	2
3. SALT PROPERTY CALIBRATION.....	5
4. FINITE ELEMENT MODELING.....	7
5. RESULTS OF FINITE ELEMENT ANALYSES.....	14
6. CALCULATION OF SURFACE SUBSIDENCE PROFILES.....	16
7. CONCLUSIONS AND RECOMMENDATIONS.....	24
8. REFERENCES.....	32
APPENDIX A Salt Mechanical Properties and Calibration	
APPENDIX B Results from Finite Element Analyses	

EXECUTIVE SUMMARY

Finite element (FE) analyses have been performed to assess the stability conditions of the 34/44 LPG storage gallery, gallery 10, well 58 and caverns 33 and 43 at the Finger Lakes facility, Watkins Glen, New York. The scope of work follows the guidelines and requirements provided by the International Gas Consulting. Laboratory test data from related projects obtained by RESPEC Inc. are used to determine the mechanical and rheological properties of the Syracuse salt and the overburden rocks. It is assumed that the tested salt cores have the same properties and behavior with those at the studied site. Conservative approach and assumptions are used in the study where applicable.

Two finite element models have been developed to represent a vertical and a horizontal cross-section of the studied galleries and caverns in relation to the site geology. Conservative cavern geometry and boundary conditions have been imposed. The analyses are made to simulate the mechanical behavior of the surrounding salt under three extreme internal pressures through the next 50 years. These cases include (1) constant hydrostatic pressure of brine, (2) the mechanical integrity test (MIT) hydrostatic pressure (about 80% of the in-situ stress at casing shoe), and (3) the minimum LPG pressure with zero wellhead pressure. The study results are summarized as follows.

- (1) The inter-cavern pillars between caverns 33 and 43, 34/44 LPG gallery and gallery 10 will be mechanically stable under the minimum LPG storage pressure of 1,197 psi at the casing shoe for the next 50 years.
- (2) The inter-cavern pillars will be mechanically stable under the MIT hydrostatic pressure of 1,680 psi at the casing shoe for the next 50 years. The MIT pressure is lower than the predicted pillar stresses.
- (3) Leakage or communication between galleries and caverns under the MIT and minimum pressures is very unlikely.
- (4) The impact of the pressure cycle is very small due to the small difference between the magnitudes of the maximum and minimum storage pressures of the LPG.
- (5) The salt pillars have been subjected to large shear strains during brine storage/production. These strains are however significantly reduced by the increase of the confining pressures in the salt pillars when the caverns/galleries are under MIT pressure and LPG storage.
- (6) Even though conservative approach, assumptions and boundary conditions have been applied in this analysis, uncertainties of the results may exist with regard to the representativeness of the salt properties and the geometry of gallery 10. However, "Since no cavern was found during the recent sonar and cement bond well logging of well 52, our conservative FE study approach appears to have been correct.
- (7) Both well 58 (far away and not on FEA map, and NYSEG Galleries 1 natural gas storage service), and 2 are also too far away to have any affect on the Finger Lakes (FL) LPG storage caverns.
- (8) Based on the results of the analyses on these large galleries with small inter-cavern pillars, Well 58 (in the same salt formation/properties/depth) is likely to be mechanically stable. This is because it is relatively small and isolated from the rest of the caverns and galleries (the inter-cavern pillar is over 1000 ft).
- (9) Well 33 will not increase in diameter if and when it is put into LPG storage service since any 30% increase in solution mining by undersaturated brine product displacement will take place above the existing maximum diameter.

- (10) Wells 43, 34, and 44 will be monitoring wells and will not be solution mined. i.e. those wells have no affect on the modeling.

1. INTRODUCTION

Finite element (FE) analyses have been performed to assess the stability conditions of the 34/44 LPG storage gallery, gallery 10, well 58 and caverns 33 and 43 at the Finger Lakes facility, Watkins Glen, New York. The study concentrates on the mechanical integrity of the inter-cavern pillars while the 34/44 LPG gallery and caverns 33 and 43 are being operated for storage. The impacts of other surrounding caverns in the facility are assessed where applicable. The scope of work follows the guidelines and requirements provided by the International Gas Consulting. A viscoelastic-viscoplastic finite element code (GEO) with strain-softening (brittle failure) function and inelastic dilation function has been used to simulate the mechanical behavior of Syracuse salt. Laboratory test data from a related project obtained by RESPEC Inc. are used to calibrate the mechanical and rheological properties of the salt and the overburden rocks. Supplementary theories and concepts on salt mechanics, as well as in-house experience and database have been applied in the analysis where applicable. The specific objectives of the analyses are as follows.

- a. Calibrate the site-specific salt properties using the laboratory mechanical test data obtained by RESPEC Inc.;
- b. Construct horizontal and vertical representative FE models for the 34/44 LPG gallery and gallery 10 of the Finger Lakes facility;
- c. Evaluate the stability of the LPG gallery under constant brine pressure and under the MIT hydrostatic pressure and minimum LPG storage pressures for the next 50 years;
- d. Evaluate the mechanical stability of well 58;
- e. Determine the mechanical stability of the inter-cavern pillars; and
- f. Predict the ultimate surface subsidence of the cavern field.

This report describes the methods and results of finite element analyses. The executive summary highlights the results with main emphases on the design recommendations. Section one defines the objectives of the study. The site-geology and cavern geometry and depth used in the model are briefly described in section two. Section three summarizes the results of the calibration of the Syracuse salt mechanical properties and the properties of the overburden rocks obtained from RESPEC. The fourth section shows the vertical and horizontal FE models constructed to represent the gallery geometry and the surrounding rocks. Section five presents the results of the FE analyses. The ultimate surface subsidence of the cavern field predicted by using Salt_SUBSID program is given in section six. Section seven concludes the results and provides design recommendations. References cited in the report are listed in section eight.

Appendix A summarizes the results of the salt property calibration using RESPEC test data. Appendix B shows the principal stress and strain distributions around the LPG storage gallery.

2. SITE AND CAVERN CHARACTERISTICS

Figure 1 shows a plan view of the Finger Lakes storage facility. This study concentrates on the mechanical behavior of the salt around the 34/44 LPG storage gallery, gallery 10 and caverns 33 and 43, located in the middle of the plan view. For this analysis the group of these galleries and caverns can be isolated from the southern NYSEG Galleries 1 and 2 and from the eastern row of caverns because they are too far away and do not have any impact on the studies area. The [REDACTED] to have any impact on the studied galleries and caverns.



Figure 1. A plan view showing cavern layout of the studied caverns 33 and 43, 34/44 LPG gallery and gallery 10 of Finger Lakes facility.

Rock sequences in the storage facility are defined here as 9 main units; (from top-to-bottom) top sediment, Tully limestone, Marcellus shale, Onondaga limestone, Helderburg/Manlius limestone, Rondout limestone, Bertie limestone, Camillus shale, and Syracuse salt. The mechanical properties of these units are discussed in the following section. Figure 2 shows thickness and depth of these rock units in relation to the casing shoe depths for the studied caverns and galleries. Since the [REDACTED] is not available at the time of this study, its [REDACTED] is assumed to be an up-right cylinder with a maximum diameter of [REDACTED] (taken from the plan view projection in Figure 1). Depths of the [REDACTED] are conservatively assumed to be the same as those of the 34/44 LPG gallery.




Figure 2. Rock sequence and profiles of (from left to right) caverns 33 and 43, 34/44 LPG gallery and gallery 10 of Finger Lakes facility.

3. SALT PROPERTY CALIBRATION

The mechanical properties of Syracuse salt used in this study are calibrated from the results of laboratory testing performed by RESPEC, Inc. (Pfeifle, 1996). The tests were conducted on the salt cores obtained from well no. 58 (of AKZO Nobel Salt Inc.) and from well no. 59 (of NYSEG) for the Seneca Lake Storage Project, Watkins Glen, New York. These results were also used in the mechanical analyses of the natural gas storage galleries 1 and 2 by Osnes and Eyermann (1996) and Skaug and Nieland (2002), respectively. The results used in this study are taken from the triaxial compressive strength tests, Brazilian tensile strength test, and triaxial creep tests. They are used to determine and calibrate the elastic parameters (Young's modulus and Poisson's ratio), and the visco-elastic and visco-plastic parameters of the salt.

Table 1 summarizes the basic mechanical properties of the salt taken from RESPEC (Pfeifle, 1996). Appendix A provides the results of calibration on the creep properties of the Syracuse salt. The Brazilian tensile strength of the salt cores from well nos. 58 and 59 is [REDACTED] compared to that of other salts (Figure A-1, Appendix A). The elastic modulus and Poisson's ratio are [REDACTED] respectively. They are compared with salt from other sources in Figures A-2 and A-3 (in Appendix A). The salt strengths are presented in form of the octahedral shear as a function of mean stress in Figure 3 with detailed calculation provided in Table A-1. They will be used to evaluate the mechanical stability of the salt in the computer simulation.

The shear modulus (G_1) and bulk modulus (K_1) of the Syracuse salt are calculated from the elastic modulus and Poisson's ratio indicated above. Detailed calculations are provided in Table A-2 of Appendix A. The visco-elastic parameters (G_2 , K_2 and η_2) and the visco-plastic coefficient (η_4) are calibrated from the triaxial creep testing (Tables A-3 and A-4). Comparisons of the predicted (calibrated) curve with the actual test measurements are given in Figure A-5 for salt cores from well no. 58 and in Figure A-6 for salt cores from well no. 59.

[REDACTED] The elastic, visco-elastic and visco-plastic parameters of the Syracuse salt are summarized in Table 2. They will be used to determine the creep behavior of the salt.

[REDACTED]

Table 1. Summary of basic mechanical properties of Syracuse salt from well no. 58 and no. 59, Seneca Lake Storage Project, Watkins Glen (Pfeifle, 1996).

Basic Mechanical Properties	Values
Brazilian tensile strength test (BRZ)	[REDACTED]
Elastic modulus (E)	[REDACTED]
Poisson's Ratio (ν)	[REDACTED]

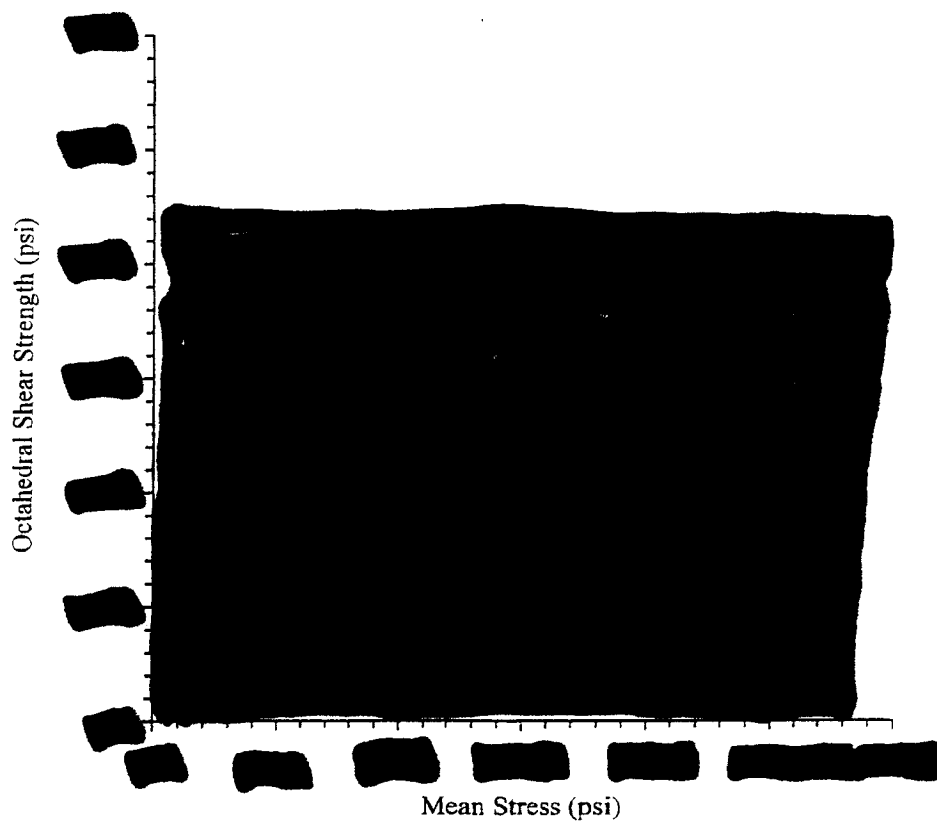


Figure 3. Salt strength data from RESPEC and the proposed strength criterion (dash line) presented in form of octahedral shear stress as a function of mean stress.

Table 2. Summary of properties parameters used in FE analyses.

Parameters	Symbols	Units	From Test	Skaug and Nieland (2002)		
			Syracuse salt	group*	group**	Shale
Elastic	E					
	ν	-				
	G_1					
	K_1					
Visco-Elastic	G_2					
	K_2					
	η_2					
Visco-Plastic	η_4					
Critical Shear Strain	γ_c					
Density gradient	γ_d					

* [REDACTED]

** [REDACTED]

4. FINITE ELEMENT MODELING

A vertical model and a horizontal model are developed in this analysis. The studied gallery and cavern shapes and layout are highly irregular. Constructing a FE model to represent [REDACTED] will be very impractical. To [REDACTED] of a representative model a [REDACTED] gallery and [REDACTED] for both vertical and horizontal models (see Figures 2 and 4). As a result the two models represent only [REDACTED] as shown in Figures 2 and 4. The presence and impact of the [REDACTED] on these galleries are incorporated as a [REDACTED] models. This approach is considered very conservative because the diameter and volume of the [REDACTED]. The analyses are made here in [REDACTED] are assumed to be [REDACTED]. Comparisons of the results from the two models will allow a redundant check on the suitability of the assumptions and the correctness of the computation.

Figure 5 shows the FE mesh for the vertical model representing the 34/44 LPG gallery and gallery 10 in relation to the depths of the rock units. The elements inside the galleries are not drawn in order to clearly show their profiles. All rock units are assumed to be in

horizontal. The [REDACTED] from the mesh boundary

[REDACTED]

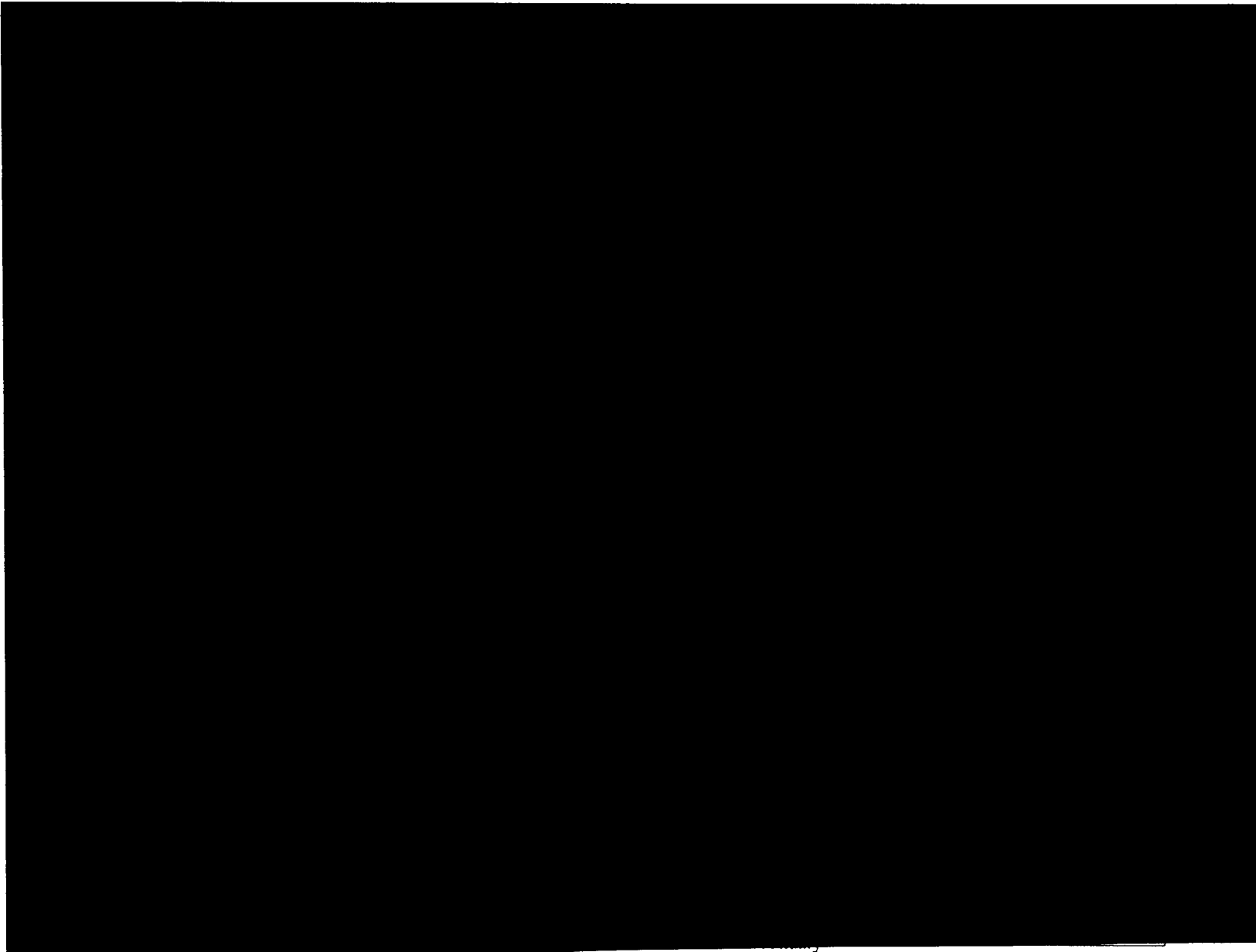


Figure 4. Horizontal cross section of the studied caverns 33 and 43, 34/44 LPG gallery and gallery 10 at depth of 2,300 ft, compared with the boundary of the horizontal model. All modeling based on deviated casing seat locations.

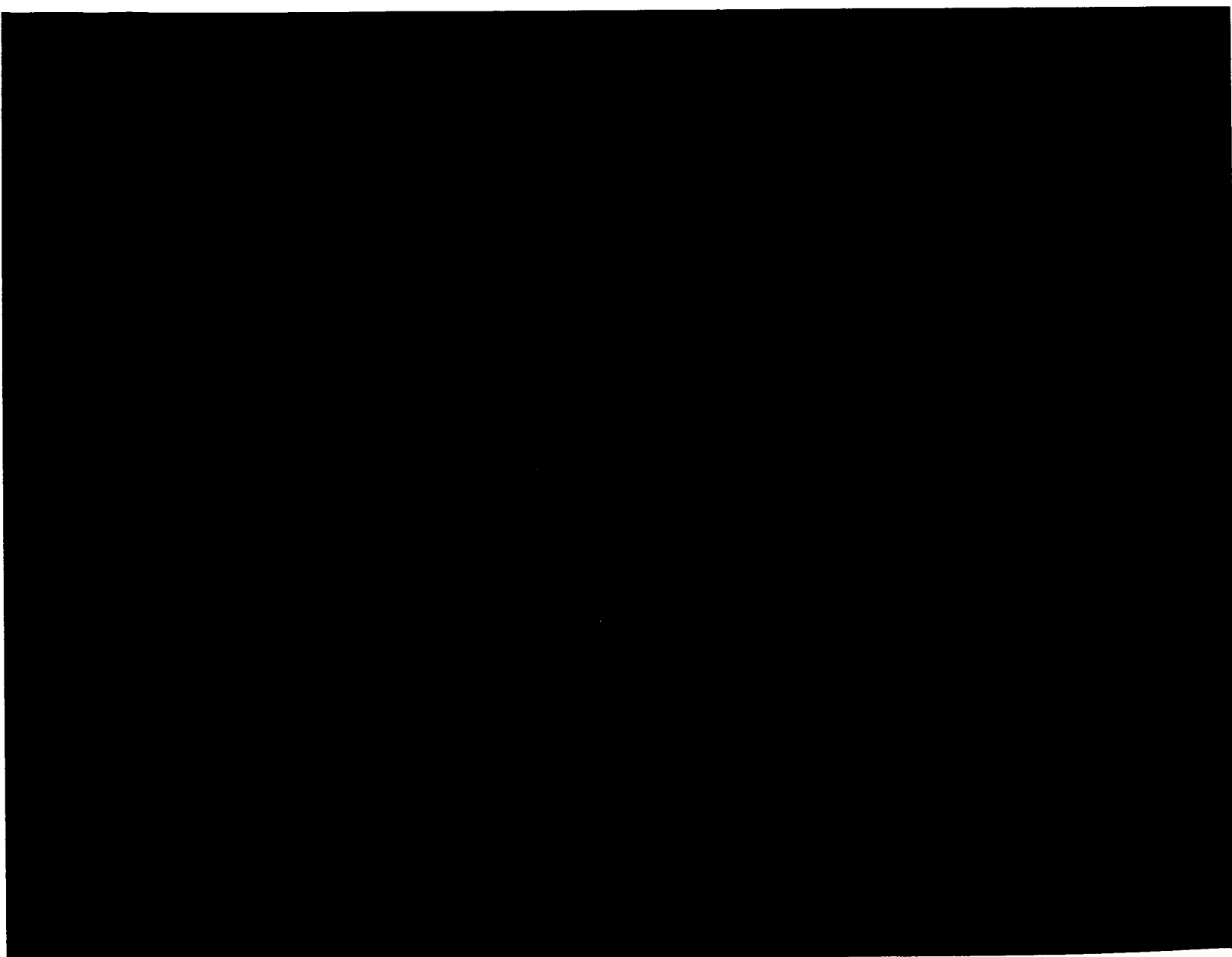


Figure 5. Finite element mesh constructed for the vertical model. The LPG (34/44) gallery on the left and [REDACTED]

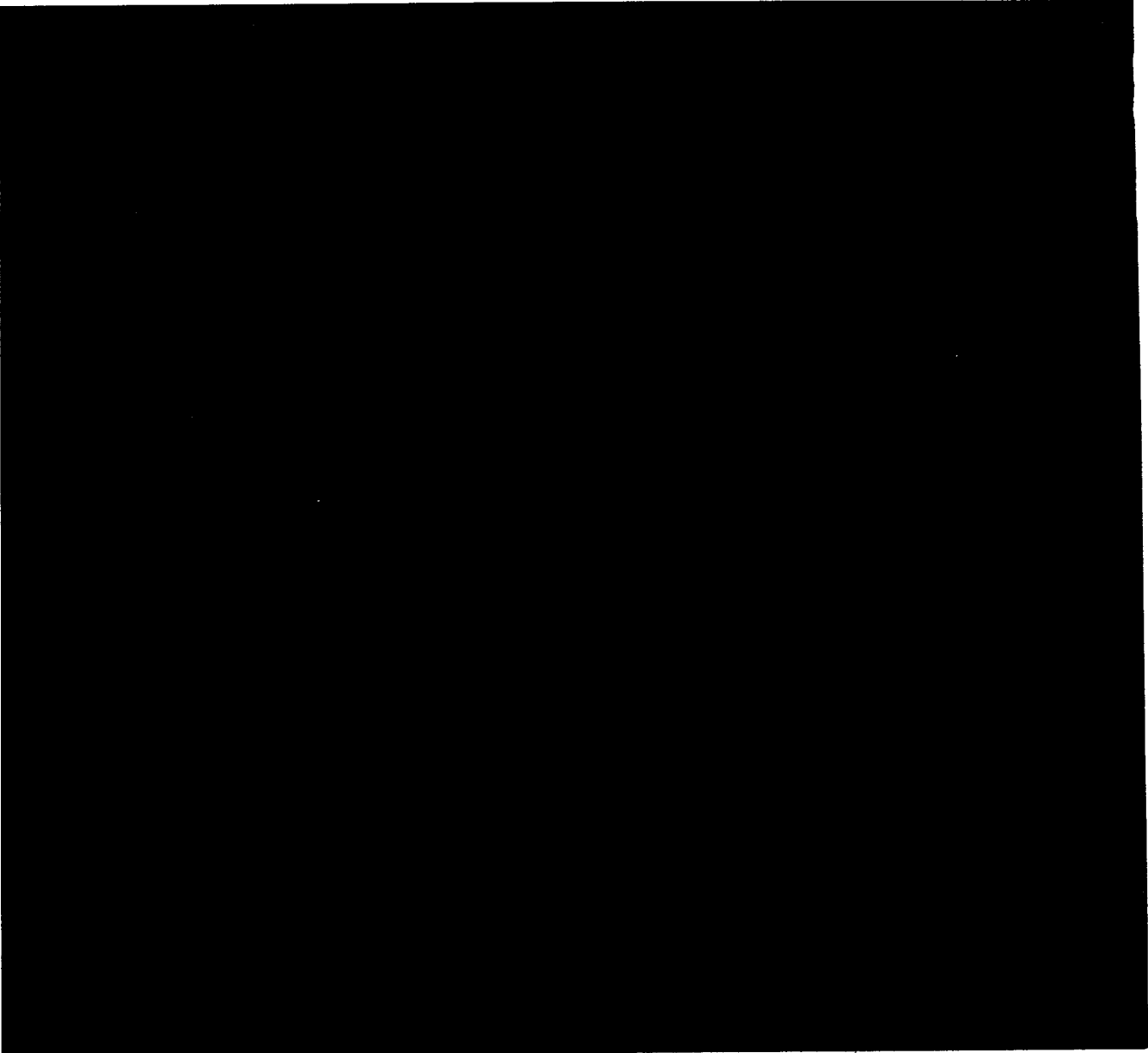
The wall-to-wall spacing between the [REDACTED] The casing shoe depth for the gallery and cavern models is taken here as [REDACTED] Since the sonar survey results [REDACTED] its vertical profile is [REDACTED] The analysis for the vertical model is in [REDACTED] into the vertical model analysis. Figure 6 shows how the [REDACTED] and [REDACTED] represent the caverns and galleries in the south. The model assumes hydrostatic in-situ stress state in the salt and overburden rocks.

Figure 7 shows the FE mesh for the horizontal model representing a horizontal profile of the 34/44 LPG gallery and gallery 10 at depth of 2,300 ft. At this depth the [REDACTED] The cavern/gallery spacings defined here are the same as those of the vertical model. The top, bottom and left boundaries are constrained while the right boundary is subject to a [REDACTED] gallery reflected by the model [REDACTED] The analysis is made in [REDACTED] It is also assumed that all caverns and galleries are excavated simultaneously.

The finite element code GEO is used in the model simulation. Figure 8 shows the modular components in the constitutive equations of GEO code. GEO is capable of describing the elastic, visco-elastic, visco-plastic, strain-softening and dilation behavior of geological materials (Fuenkajorn and Serata, 1993, 1994; Serata and Fuenkajorn, 1992; Stormont and Fuenkajorn, 1994). The code has been previously used to analyze mechanical stability of several brine and gas storage caverns in rock salt (e.g. for International Gas Consulting, Inc., Amoco, World Bank, Mississippi Hub, Inergy Savona and Unocal Corporation).

In summary the development of the vertical and horizontal models in terms of size, shape and location of the studied cavern/gallery and their surrounding caverns is based on the following conservative assumptions.

- (1) For the vertical model, [REDACTED] (perpendicular to the simulated plane) with a maximum diameter of [REDACTED] and the height equal to that of the [REDACTED] This is called plane strain analysis – reducing the three-dimensional geometric problem into a conservative two-dimensional geometry. As a result the size and volume of [REDACTED] modeled here would be much larger than the actual. [REDACTED]



[REDACTED]

caverns and galleries in vertical model.

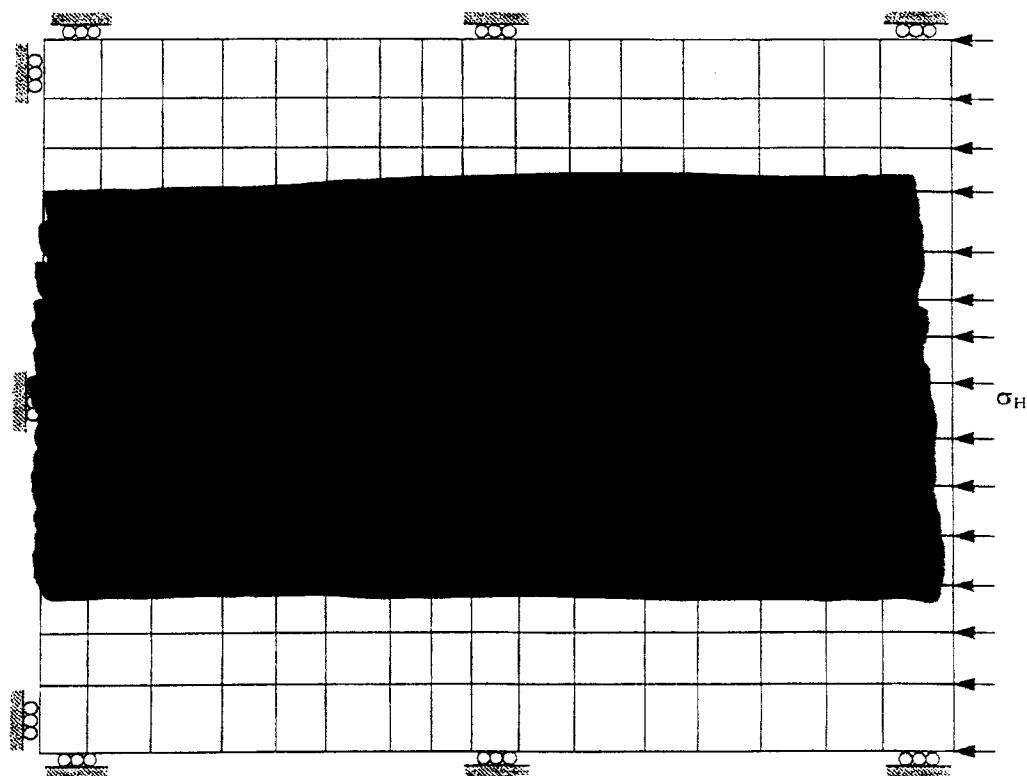


Figure 7. Finite element mesh for horizontal model representing a horizontal cross section at 2,300 ft depth. The 34/44 LPG gallery on the left and brine gallery 10 on the right. The applied

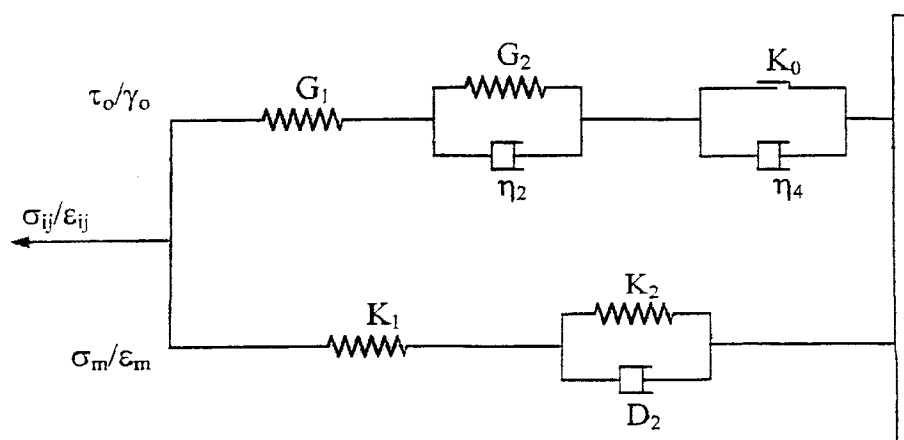


Figure 8. Modular representation of constitutive equations for rock salt in finite element program GEO (modified from Serata and Fuenkajorn, 1993).

- (4) Figure 6 shows how the Galleries 1 and 2 and well 58 are incorporated into the modeling. Their location and size are [REDACTED] by the [REDACTED] which is modeled as a [REDACTED]. This is considered highly conservative because the [REDACTED] is [REDACTED] than those of the [REDACTED].
- (5) Similarly for the horizontal model (see also Figure 4) the impact of the [REDACTED] and gallery is conservatively analyzed by using the [REDACTED]. The horizontal model also assumes that [REDACTED] with axis perpendicular to the analyzed plane. This imposes the most severe condition in terms of the cavern shape.
- (6) The internal pressures for Gallery 10 and 34/44 Gallery assumed in the vertical and horizontal models are also [REDACTED]. Since the two galleries are larger than those [REDACTED] the impact of the simulated pressures will be [REDACTED]. Details of the simulated pressures are described below.

Three extreme scenarios for the cavern/gallery pressures are assumed for the analyses of the vertical and horizontal models. These simulated pressures impose the most severe stress conditions to the surrounding salt. All cases are simulated through the next 50 years.

Case 1: Constant hydrostatic pressure of brine. Caverns 33 and 43, 34/44 gallery and gallery 10 are subject to a constant hydrostatics pressure of brine for 50 years. For the vertical model the internal pressure at their casing shoe is [REDACTED]. The pressure linearly increases at the gradient of [REDACTED] from the top to the bottom of the caverns/galleries. For the horizontal model simulated at [REDACTED] depth the internal pressure for all caverns and galleries are [REDACTED].

Case 2: Constant maximum MIT hydrostatic pressure in caverns 33 and 43 and 34/44 LPG gallery. For the vertical model the internal pressure at the casing shoe is [REDACTED] of the stress at casing shoe). The pressure increases at the gradient of [REDACTED] from the top to the bottom of the caverns [REDACTED]. Gallery 10 [REDACTED]. For the horizontal model the 34/44 LPG gallery and the two caverns are subject to a constant internal pressure of [REDACTED] depth of [REDACTED] plus brine pressure gradient of [REDACTED] to the depth of [REDACTED]. Gallery 10 is under the [REDACTED].

Case 3: Constant minimum LPG pressure in caverns 33 and 43 and 34/44 LPG gallery. The internal pressure at the casing shoe for the vertical model is [REDACTED] and increases linearly at the gradient of [REDACTED] from the top to the bottom of the caverns 33 and 43 and 34/44 LPG gallery. Gallery 10 [REDACTED]. For the horizontal model the 34/44 LPG gallery and the two caverns are subject to a constant internal pressure of [REDACTED].

[REDACTED]

[REDACTED]

[REDACTED]

5. RESULTS OF FINITE ELEMENT ANALYSES

5.1 Vertical Model Results

The principal stress distributions obtained from all three simulated cases indicate that [REDACTED] and [REDACTED]. All stresses are [REDACTED]. This suggests that the [REDACTED] is safe. Figures B-1 through B-3 (Appendix B) shows the principal stress vectors calculated in the salt around the caverns and galleries.

The calculated principal strain vectors in the salt pillars show that the largest pillar deformation occurs when the galleries are [REDACTED]. The maximum MIT pressure simulation shows the [REDACTED] (see Figures B-4 through B-6, Appendix B). The [REDACTED] between [REDACTED] are plotted as a function of time in Figure 9 when all galleries and caverns are subject to the hydrostatic pressure of brine which represents the [REDACTED]. The deformation curves, nevertheless, indicate that these [REDACTED]. This implies that the [REDACTED] and the [REDACTED] in the 34/44 gallery will also be [REDACTED]. This is supported by the [REDACTED] (shown in Figures 10 and 11) that [REDACTED] will occur during the [REDACTED]. Beyond [REDACTED]

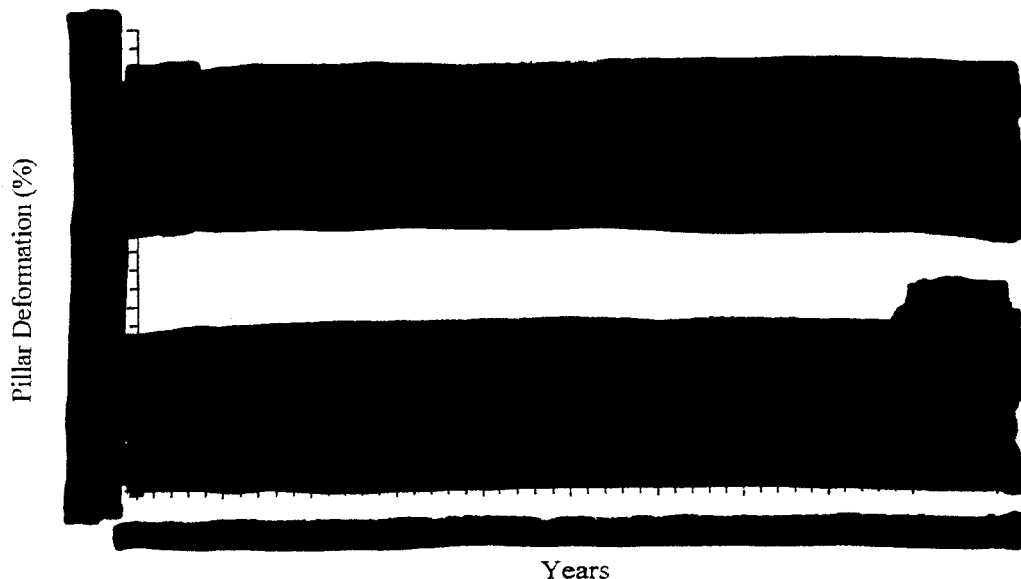


Figure 9. Horizontal deformation of salt pillar when both galleries are under hydrostatic pressure of brine for 50 years, (1) between cavern 43 and 34/44 LPG gallery, (2) between 34/44 LPG gallery and gallery 10.

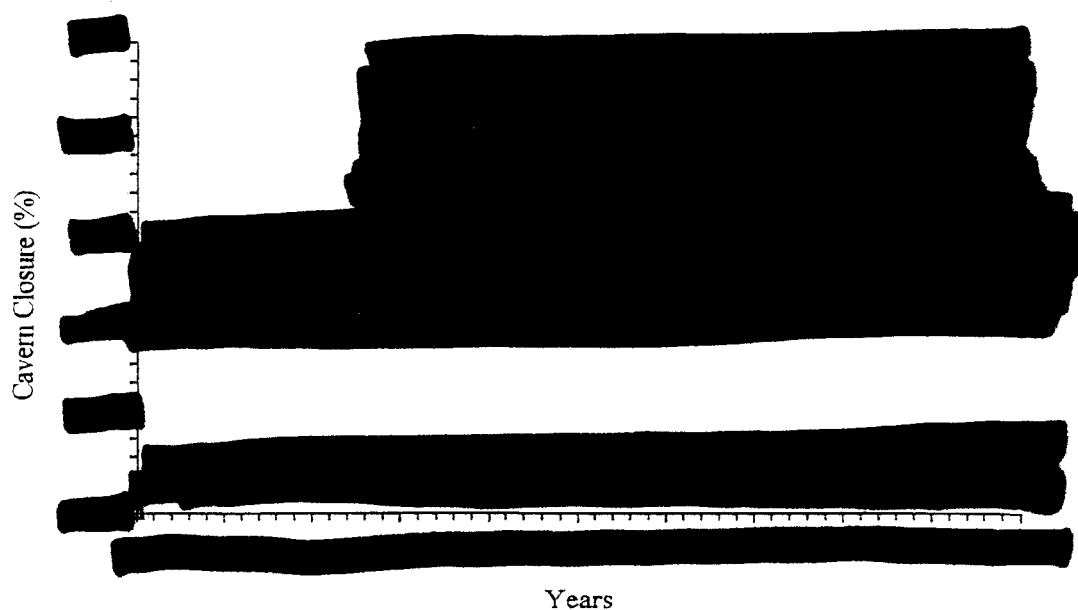


Figure 10. Vertical and horizontal closure of the 34/44 LPG gallery when both galleries are under hydrostatic pressure of brine for 50 years.



Figure 11. Surface subsidence above 34/44 LPG gallery when both galleries are under hydrostatic pressure of brine for the next 50 years.

To assess the hydrological containment of the studied galleries and caverns the octahedral shear strains induced in the surrounding salt for cases 1 and 2 are calculated and plotted in a form of representative contours in Figures 12 and 13. The results show that when [REDACTED] are [REDACTED], the salt pillars between them [REDACTED] see Table 2). This implies that [REDACTED]. This is due to the [REDACTED] compared to [REDACTED]. These [REDACTED] however [REDACTED] when the galleries/caverns are [REDACTED]. The [REDACTED] are closer to the [REDACTED]. As a result, the [REDACTED] should not become [REDACTED] because when the galleries/caverns are operating, the [REDACTED] in the [REDACTED]. Figures 14 and 15 show the mean stresses in the salt pillars when the galleries/caverns are under brine hydrostatic pressure and MIT pressure, respectively.

5.2 Horizontal Model Results

The [REDACTED] obtained from all three simulated cases in the horizontal model indicate that [REDACTED] is induced in the [REDACTED]. All [REDACTED] implying that [REDACTED] when the [REDACTED] is applied (Figures B-7 through B-9). This confirms the vertical model results above that for all cases the [REDACTED]. The horizontal model results also [REDACTED] with those of the vertical model that the [REDACTED] in the [REDACTED] induces [REDACTED] than do the [REDACTED] (compare Figures B-10 through B-12).

Similar to the vertical model simulations above, the induced octahedral shear strains and mean stresses in the salt pillars for cases 1 and 2 of the horizontal model are calculated to assess the hydrological containment of the galleries/caverns, as shown in Figures 16 through 19. The results [REDACTED]. The [REDACTED] in the [REDACTED] when the caverns/galleries are under [REDACTED].

The [REDACTED]

due to the [REDACTED]

As a result, [REDACTED]

6. CALCULATION OF SURFACE SUBSIDENCE PROFILES

The SALT_SUBSID code was developed by RE/SPEC Inc. (Nieland, 1991) and is used to predict the three-dimensional surface subsidence for the Finger Lakes LPG storage field. There are [REDACTED] included in this calculation. Table 3 lists the drilling dates and volume of these wells which are used as data input for the Salt_SUBSID code. The code can calculate the subsidence profile induced by dry mining (underground openings) and solution mining (brine caverns).

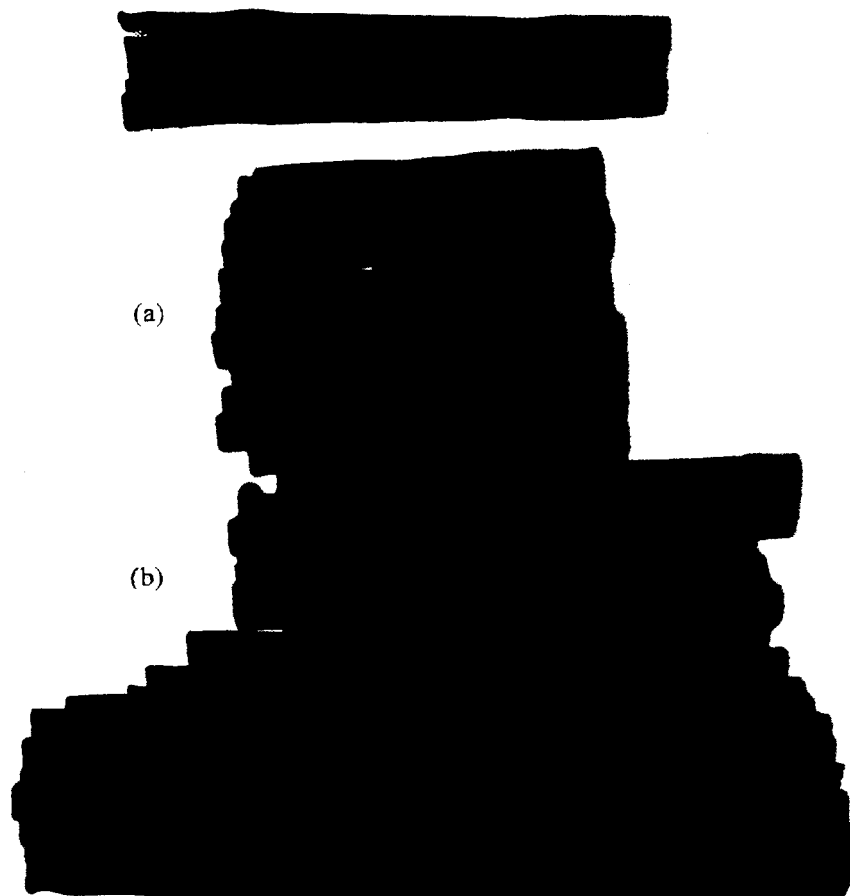


Figure 12. Contour of octahedral shear strain in salt pillars when both galleries are under hydrostatic pressure of brine for 50 years. (a) Pillar between cavern no. 43 and 34/44 LPG gallery. (b) Pillar between 34/44 LPG gallery and gallery 10.

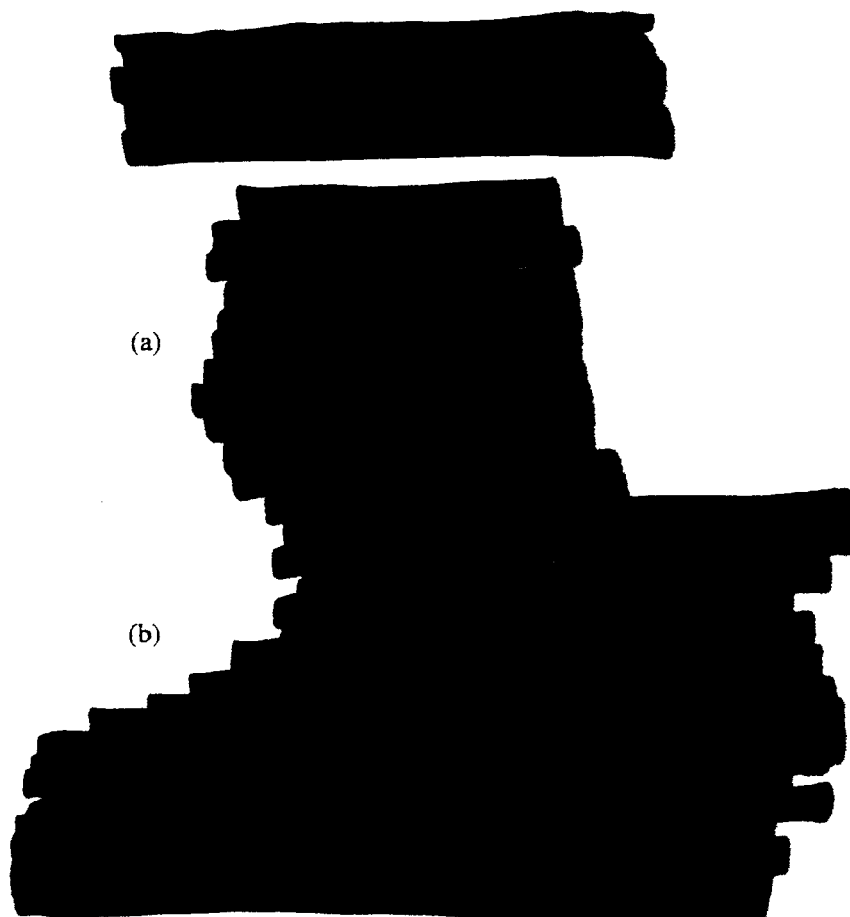


Figure 13. Contour of octahedral shear strain in salt pillars when 34/44 LPG gallery is under MIT pressure and gallery 10 is under hydrostatic pressure of brine at year 50. (a) Pillar between cavern no. 43 and 34/44 LPG gallery. (b) Pillar between 34/44 LPG gallery and gallery 10.

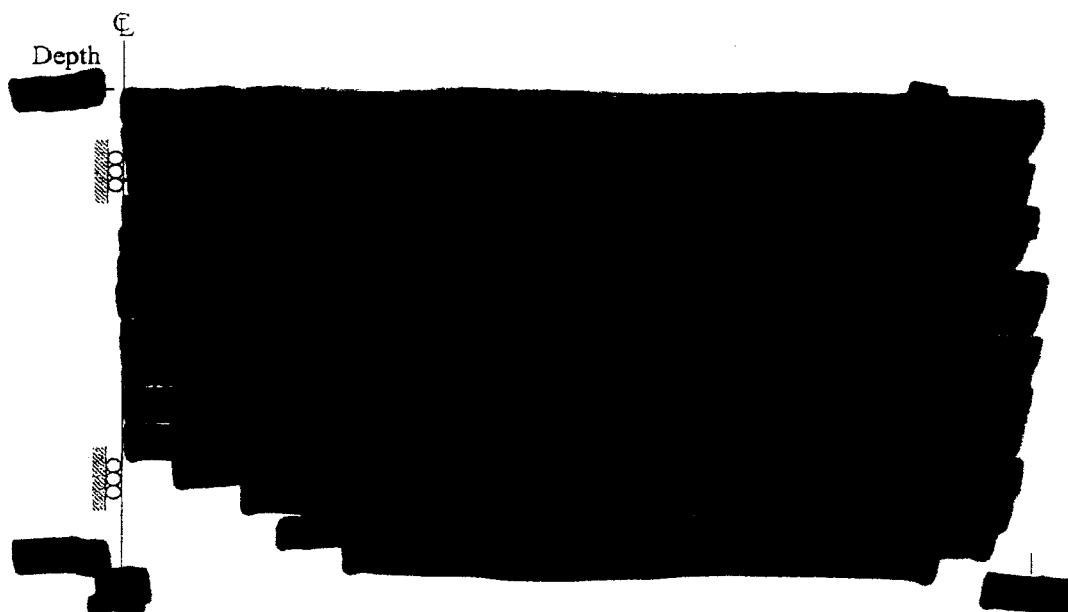


Figure 14. Contour of mean stress in salt pillars when both galleries are under hydrostatic pressure of brine for 50 years. Contour interval = [REDACTED]

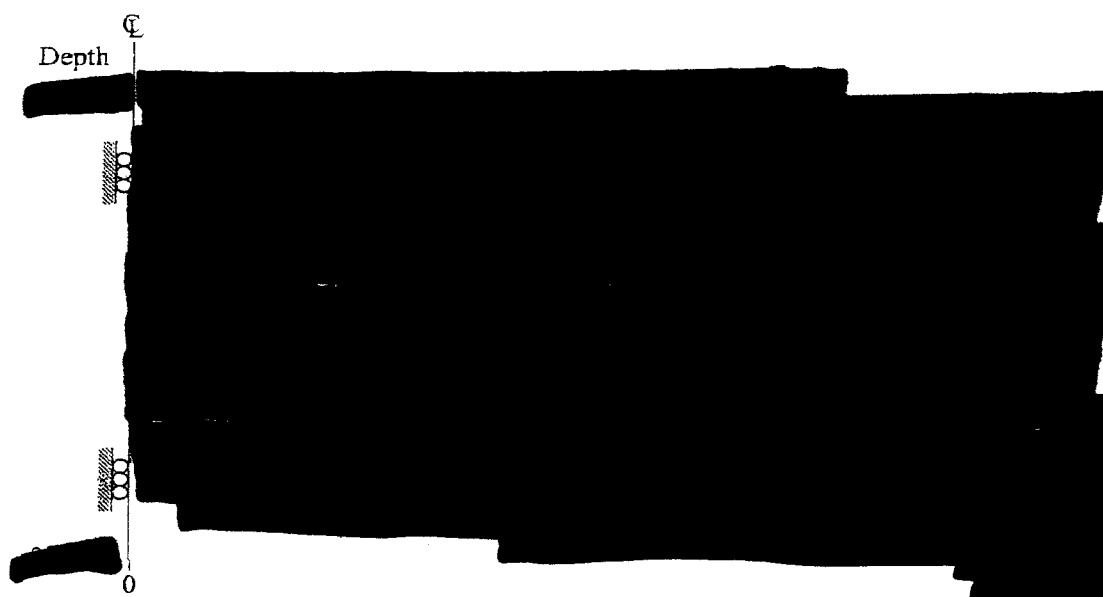


Figure 15. Contour of mean stress in salt pillars when 34/44 LPG gallery is under MIT pressure and gallery 10 is under hydrostatic pressure of brine at year 50. Contour interval = [REDACTED]

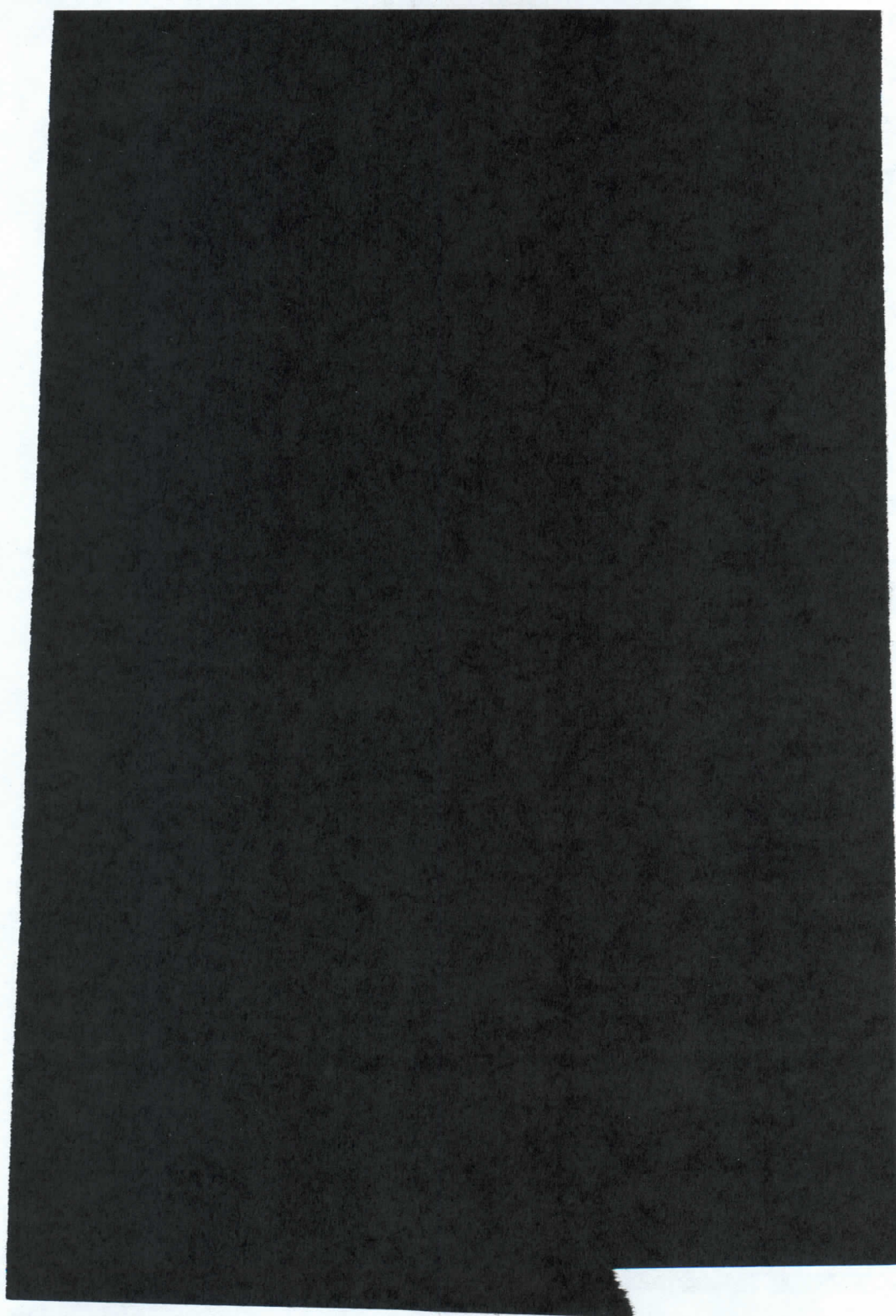


Figure 16. Contour of octahedral shear strain in salt pillars from horizontal model, simulated for both galleries that are under hydrostatic pressure of brine for 50 years. (a) Pillar between cavern no. 43 and 34/44 LPG gallery. (b) Pillar between 34/44 LPG gallery and gallery 10.

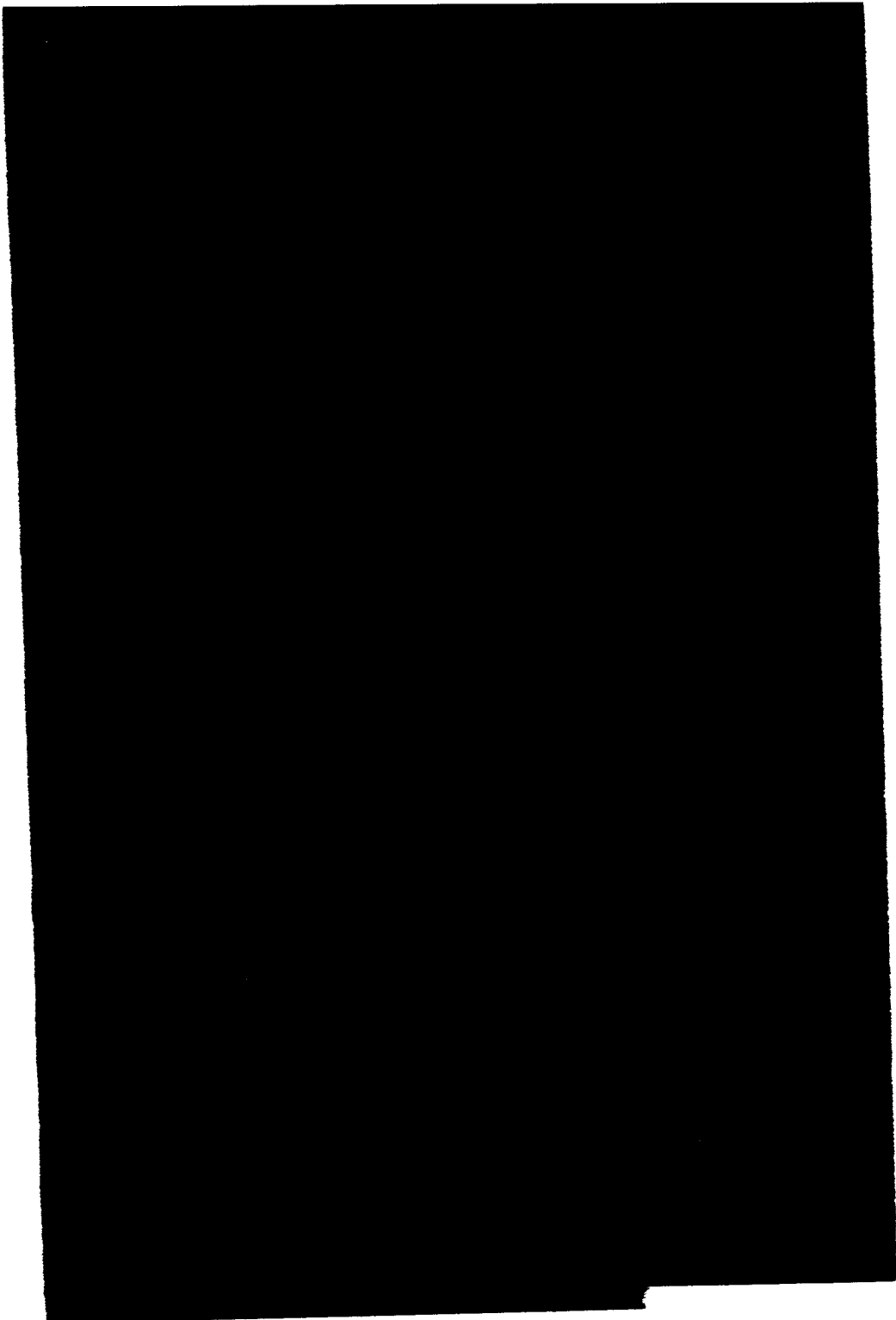


Figure 17. Contour of octahedral shear strain in salt pillars from horizontal model. The 34/44 LPG gallery is under maximum MIT pressure and gallery 10 is under hydrostatic pressure of brine at year 50. Contour interval = [REDACTED] (a) Pillar between cavern no. 43 and 34/44 LPG gallery. (b) Pillar between 34/44 LPG gallery and gallery 10.

Figure 18. Contour of mean stress in salt pillars from horizontal model, simulated for both galleries are under hydrostatic pressure of brine for 50 years. Contour interval =

Figure 19. Contour of mean stress in salt pillars from horizontal model. The 34/44 LPG gallery is under MIT pressure and gallery 10 is under hydrostatic pressure of brine at year 50. Contour interval = [REDACTED]

Table 3. Drilling date and volumes of wells in studied area.

Well No.	Drilling Dates	Volume (ft ³)
Well 35	1963	[REDACTED]
Well 36	1963	[REDACTED]
Well 37	1964	[REDACTED]
Well 38	1964	[REDACTED]
Well 41	1966	[REDACTED]
Well 40	1965	[REDACTED]
Well 42	1966	[REDACTED]
Well 47	1972	[REDACTED]
Well 48	1972	[REDACTED]
Well 50	1972	[REDACTED]
Well 51	1972	[REDACTED]
Well 55	1967	[REDACTED]
Well 56	1977	[REDACTED]
Well 33	1972	[REDACTED]
Well 34	1971	[REDACTED]
Well 44	1967	[REDACTED]
Well 43	1966	[REDACTED]
Well 18	1963	[REDACTED]
Well 52	1972	[REDACTED]
Well 57	1977	[REDACTED]
Well 58	1992	[REDACTED]
Well 60	2003	[REDACTED]
Well 61	1999	[REDACTED]
Well 62	2008	[REDACTED]
Well 30	1995	[REDACTED]
Well 45	1995	[REDACTED]
Well 31	1995	[REDACTED]
Well 28	1995	[REDACTED]
Well 59	1995	[REDACTED]
Well 46	1995	[REDACTED]
Well 27	1995	[REDACTED]
Well 33*	2010	[REDACTED]
Well 34*	2010	[REDACTED]
Well 43*	2010	[REDACTED]
Well 58*	2010	[REDACTED]

*increase of the storage volume by [REDACTED]

The key parameters used in SALT_SUBSID have been calibrated using the subsidence results computed by the finite element analysis presented in the previous section. This approach will make the predicted subsidence profile over the storage field more site-specific. Results from the calibration of these key parameters for the Finger Lakes storage field are as follows; [REDACTED] and [REDACTED]. Definition of these parameters is described in details by Nieland (1991).

The subsidence profiles are calculated for year 1963 through year 2060 (next 50 years). The [REDACTED] after well development. [REDACTED] The [REDACTED] to the present day due to the [REDACTED]. Additional [REDACTED] is predicted from [REDACTED] due to the increase of the [REDACTED]. Beyond year 2016 through 2060 the [REDACTED]. With the maximum magnitudes of about [REDACTED] above [REDACTED], and about [REDACTED] above [REDACTED]. Figures 20 through 25 show surface subsidence contours of the Finger Lakes storage field for years 1980, 1990, 2000, 2010, 2012, and 2016 through 2060. The north-south profiles of surface subsidence for various periods are plotted in Figure 26.

7. CONCLUSIONS AND RECOMMENDATIONS

Two finite element models were developed to represent a vertical and a horizontal cross-section of the 34/44 LPG gallery, gallery 10 and cavern nos. 33 and 43 of the Finger Lakes facility, Watkins Glen, New York. The models represent the most conservative geometry and layout of the studied galleries/caverns. The analyses are made to simulate the mechanical behavior of the surrounding salt under three extreme internal pressures through the next 50 years. The three cases include (1) constant hydrostatic pressure of brine, (2) the MIT hydrostatic pressure, and (3) the minimum LPG pressure with zero wellhead pressure. The study results are summarized as follows.

1. The inter-cavern pillars between caverns 33 and 43, 34/44 LPG gallery and gallery 10 will be mechanically stable under the minimum LPG storage pressure of 1,197 psi at the casing shoe for the next 50 years.
2. The inter-cavern pillars will be mechanically stable under the MIT hydrostatic pressure of 1,680 psi at the casing shoe (80% of in-situ stress) for the next 50 years. The LPG pressures and the MIT pressure are lower than the predicted pillar stresses.
3. Leakage or communication between galleries and caverns under the MIT pressure and the minimum LPG pressure is very unlikely.
4. The impact of the pressure cycle is very small due to the small difference between the proposed magnitudes of the maximum and minimum storage pressures of the LPG.
5. The salt pillars have been subjected to large shear strains during brine storage/production. These strains are however significantly reduced by the increase of the confining pressures in the salt pillars when the caverns/galleries are under MIT pressure and LPG storage.



Figure 20. Contour of surface subsidence at year 1980.

Figure 21. Contour of surface subsidence at year 1990.

Figure 22. Contour of surface subsidence at year 2000.

Figure 23. Contour of surface subsidence at year 2010.

Figure 24. Contour of surface subsidence at year 2012.



Figure 25. Contour of surface subsidence from year 2016 through 2060.

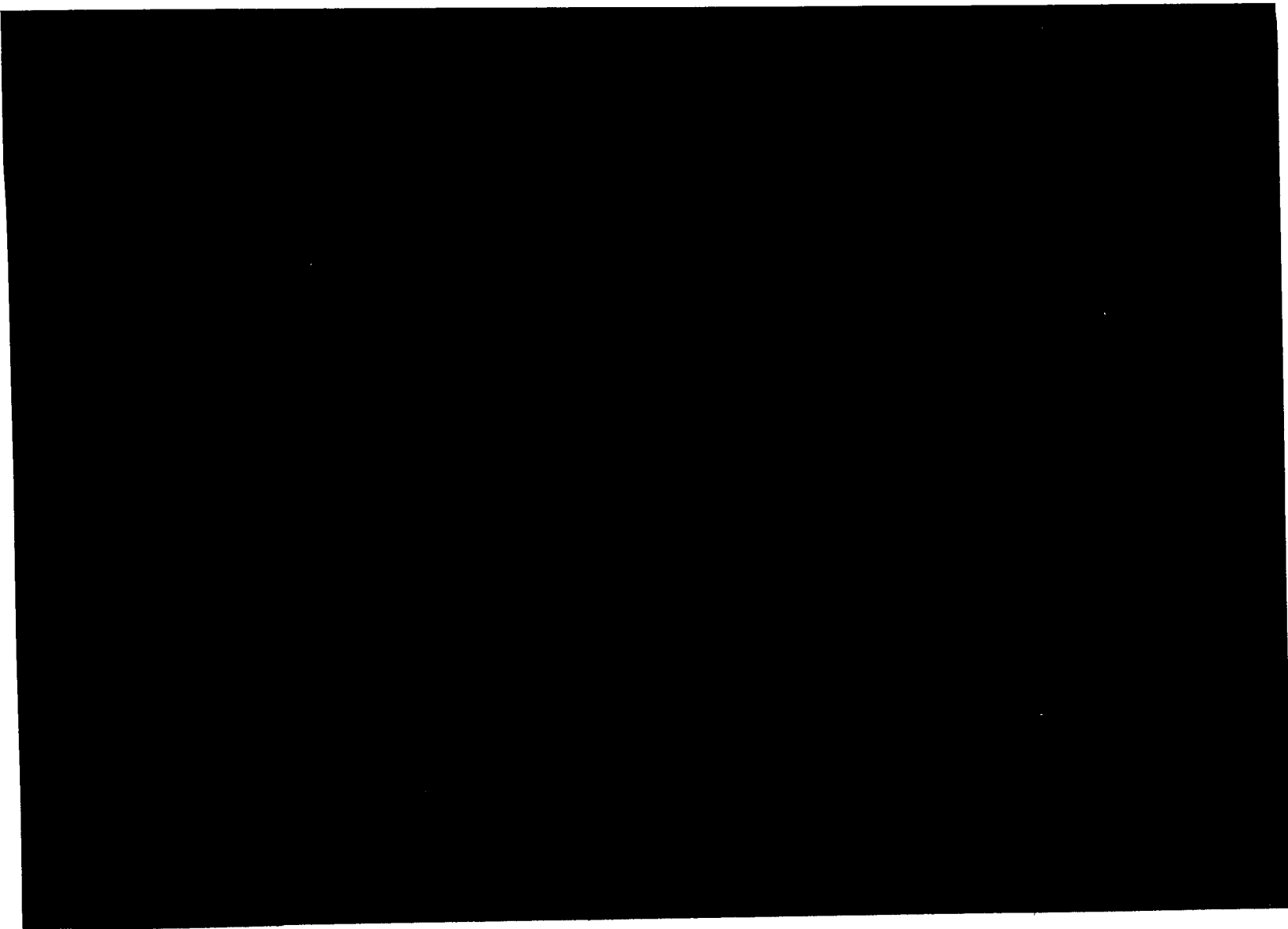


Figure 26. Subsidence profiles predicted for various periods. Vertical scale is excessively exaggerated.

6. Even though conservative approach, assumptions and boundary conditions have been applied in this analysis, uncertainties may exist with regard to the representativeness of the salt properties and the geometry of gallery 10. . However. "Since no cavern was found during the recent sonar and cement bond well logging, our conservative FE study approach appears to have been correct.
7. Both well 58 (far away and not on FEA map, and NYSEG Galleries 1 (natural gas storage service), and 2 are also too far away to have any affect on the Finger Lakes (FL) LPG storage caverns.
8. Based on the results of the analyses on these large galleries with small inter-cavern pillars, Well 58 (in the same salt formation/properties/depth) is likely to be mechanically stable. This is because it is relatively small and isolated from the rest of the caverns and galleries (the inter-cavern pillar is over 1000 ft).
9. Well 33 will not increase in diameter if and when it is put into LPG storage service since any 30% increase in solution mining by undersaturated brine product displacement will take place above the existing maximum diameter.
10. Wells 43, 34, and 44 will be monitoring wells and will not be solution mined. i.e. those wells have no affect on the modeling.

8. REFERENCES

- Boontongloan, C. (2000) *Engineering properties of the evaporitic and clastic rocks of Maha Sarakam Formation, Sakon Nakhon evaporite basin*. M.S. thesis, Asian Institute of Technology, Thailand.
- DeVries, K. L., Mellegard K. D., and Callahan G. D. (2002) *Salt damage criterion proof-of-concept research*, Topical report, DE-FC26-00NT41026, prepared for the U.S. Department of Energy, Pennsylvania.
- Fuenkajorn, K. (1997) *Design and Analysis of Gas Storage Caverns in Hutchinson Salt Formation, Kansas*, Technical Report, Prepared for the International Gas Consulting, Inc., Houston, Texas, USA, by Rock Engineering International, Tucson, Arizona.
- Fuenkajorn, K. (2005) *Design Evaluation of Canatxx Presall Gas Storage Facility*, Technical Report, Prepared for Cataxx Inc., Houston, Texas, USA, by Geomechanics Research Unite, Suranaree University of Technology, Thailand.
- Fuenkajorn, K. (2005) *Tuz Golu Underground Gas Storage Facility Finite Element Analysis*, Final Report, Prepared for International Gas Consulting Inc. Houston, Texas, USA, by Geomechanics Research Unite, Suranaree University of Technology, Thailand.
- Fuenkajorn, K. (2007) *Mississippi Hub Gas Storage Caverns: Finite Element Analysis*, Technical Report, Prepared for International Gas Consulting Inc., Houston, Texas, USA, by Geomechanics Research Unite, Suranaree University of Technology, Thailand.
- Fuenkajorn, K. (2008a) *Finite Element Analysis for Gas Storage Caverns "Joy Station Project" Kiowa County, Kansas*, Technical Report, Prepared for the International Gas Consulting, Inc., Houston, Texas, USA, by Geomechanics Research Unite, Suranaree University of Technology, Thailand.
- Fuenkajorn, K. (2008b) *Inergy Savona LPG Storage Facility: Finite Element Analysis*, Technical Report, Prepared for the International Gas Consulting, Inc., Houston, Texas,

- USA, by Geomechanics Research Unite, Suranaree University of Technology, Thailand.
- Fuenkajorn, K. (2009) *Finite Element Analysis on North Dayton Naturak Gas Storage Caverns C-1, C-2 and C-4*, Technical Report, Prepared for the International Gas Consulting, Inc., Houston, Texas, USA, by Geomechanics Research Unite, Suranaree University of Technology, Thailand.
- Fuenkajorn, K. and Daemen, J. J. K. (1988) *Borehole Closure in Salt*, Technical Report NUREC/CR-5243, prepared for the U.S. Nuclear Regulatory Commission, Washington, D.C.
- Fuenkajorn, K. and Jandakaew, M. (2003) Compressed-air energy storage in salt dome at Borabu district, Thailand: Geotechnical Aspects, *Proceedings of the 38th Symposium on Engineering Geology and Geotechnical Engineering*, University of Reno, Nevada, March 19-21, pp. 377-391.
- Fuenkajorn, K. and Serata, S. (1993) Numerical simulation of strain-softening and dilation of rock salt, *International Journal of Rock Mechanics and Mining Sciences and Geomechanics Abstracts*, 30(7), pp. 1303-1306.
- Fuenkajorn, K. and Serata, S. (1994) Dilation-induced permeability increase around caverns in rock salt, *Proceeding of the First North American Rock Mechanics Symposium*, University of Texas at Austin, June 1-3, pp. 648-656.
- GeoTesting Express, Inc. (2004) *Geotechnical Testing of Rock Specimens*, Prepared for Geocomp Consulting, August, Boxborough MA.
- Goodman, R. E. (1989) *Introduction to Rock Mechanics* (2nd ed.), Canada: John Wiley & Sons.
- Hamami, M., Tijani, S. M., and Vouille, G. (1993) A methodology for the identification of rock salt behavior using multi-steps creep tests, *Proceedings of the Third Conference on the Mechanical Behavior of Rock Salt*, Pennsylvania State University-Pennsylvania, November 1981, Trans Tech Publications, Clausthal-Zellerfeld, Germany, pp. 53-69.
- Hansen, F. D. and Carter, L. N. (1981) Creep of Avery Island rock salt, *Proceedings of First Conference on the Mechanical Behavior of Rock Salt*, Pennsylvania State University-Pennsylvania, September 1981, Trans Tech Publications, Clausthal-Zellerfeld, Germany, pp. 53-66.
- Hansen, F. D., Mellegard, K. D., and Senseny, P. E. (1984) Elasticity and strength of ten natural rock salts, *Mechanical Behavior of Salt I, Proceedings of the First Conference on the Mechanical Behavior of Salt*, The Pennsylvania State University, November 9-11, 1981, Clausthal-Zellerfeld, Federal Republic of Germany, Trans Tech Publications, pp. 71-83.
- Hunsche, U. (1981) Results and interpretation of creep experiments on rock salt, *Proceedings of the First Conference on the Mechanical Behavior of Rock Salt*, Pennsylvania State University-Pennsylvania, November 1981, Trans Tech Publications, Clausthal-Zellerfeld, Germany, pp. 159-167.
- Jaeger, J. C. and Cook, N. G. W. (1979) *Fundamentals of Rock Mechanics* (3rd ed.), London: Chapman and Hall.
- Jandakaew, M. (2003) *Experimental Assessment of Stress Path Effects on Rock Salt Deformation*, M.S. thesis, Suranaree University of Technology, Thailand.
- Nieland, J. D. (1991) *SALT SUBSID: A PC-Based Subsidence Model*, Research project report No.1991-2-SMRI, Solution Mining Research Institute.
- Osnes, J.D. and Eyermann, T.J. (1996) *Geomechanics Analyses of Compressed Natural Gas Storage in Gallery No. 1, Watkins Glenn, New York*, Topical Report RSI-0670 Prepared for PB-KBB Inc., Houston, Texas, by RE/SPEC Inc., Rapid City South Dakota.

- Pfeifle, T.W. (1996) *Mechanical Properties of Salt and Dolostone from Akzo Nobel Salt Inc. Well No. 58 and NYSEG Well No. 59, Seneca Lake Storage Project, Watkins Glen, New York*, Technical Report RSI-0668, Prepared for PB-KBB Inc., Houston, Texas, by RE/SPEC Inc., Rapid City South Dakota.
- Phueakphum, D. (2003) *Compressed-Air Energy Storage in Rock Salt of the Maha Sarakham Formation*, M.S. thesis, Suranaree University of Technology, Thailand.
- Serata, S. and Fuenkajorn, K. (1992) Finite element program GEO for modeling brittle-ductile deterioration of earth structures, *SMRI Paper, presented at the Solution Mining Research Institute, Fall Meeting*, October 19-22, Houston, Texas, 24 p.
- Skaug, N.T. and Nieland, J.D. (2002) *Geomechanical Evaluation of Natural Gas Storage in Gallery No. 2 Seneca Lake Storage Incorporated Storage Project, New York*, Topical Report RSI-1574, Prepared for PB-KBB Inc., Houston, Texas, by RE/SPEC Inc., Rapid City South Dakota.
- Stormont, J. C. and Fuenkajorn, K. (1994) Dilation-induced permeability changes in rock salt, *Proceedings of the Eight International Conferences, Computer Methods and Advances in Geomechanics*, Morgantown, West Virginia, May 22-28, pp. 1296-1273.
- Vouille, G., Tijani, S. M., and de Grenier, F. (1981) Experimental determination of the rheological behavior of tersanne rock salt, *Proceedings of the First Conference on the Mechanical Behavior of Rock Salt*, Pennsylvania State University-Pennsylvania, November 1981, Trans Tech Publications, Clausthal -Zellerfeld, Geramany, pp. 407-420.
- Wetchasat, K. (2002) *Assessment of mechanical performance of rock salt formations for nuclear waste repository in northeastern Thailand*, M.S. thesis, Suranaree University of Technology, Thailand.

APPENDIX A

Salt Mechanical Properties and Calibration



Brazilian Tensile Strength (MPa)

Figure A-1. Comparison of Brazilian tensile strengths of salt from various sources (¹Hansen et al., 1984; ²Fuenkajorn, 2008a; ³Fuenkajorn, 2008b; ⁴DeVries et al., 2002; ⁵Fuenkajorn, 2007 and ⁶Fuenkajorn, 2009).




Figure A-2. Comparison of elastic modulus of salt from various sources (¹Hansen et al., 1984; ²Fuenkajorn and Daemen, 1988; ³Fuenkajorn, 2008a; ⁴Fuenkajorn, 2007; ⁵Fuenkajorn, 2005; ⁶Fuenkajorn, 2008b and ⁷Fuenkajorn, 2009).




Figure A-3. Comparison of Poisson's ratio of salt from various sources (¹Hansen et al., 1984; ²Fuenkajorn and Daemen, 1988; ³Fuenkajorn, 2008a; ⁴Fuenkajorn, 2007; ⁵Fuenkajorn, 2005; ⁶Fuenkajorn, 2008b and ⁷Fuenkajorn, 2009). CSR – constant strain rate quasi-static strength, CMS – constant mean stress dilation test.




Figure A-4. Results of strength testing of Syracuse salt from Watkins Glen presented in form of octahedral shear and mean stresses.




Figure A-5. Comparison between the calibration curves (dashed lines) and the test results from the stages of triaxial creep tests of Syracuse salt from Well no. 58 under constant confining pressure of [REDACTED]




Figure A-6. Comparison between the calibration curves (dashed lines) and the test results from the stages of triaxial creep tests of Syracuse salt from Well no. 59 under constant confining pressure of [REDACTED]

Table A-1. Octahedral shear strengths calculated from laboratory strength testing by RESPEC Inc.

Test Methods	Sample No.	σ_1 (psi)	σ_2 (psi)	σ_3 (psi)	σ_m (psi)	τ_{oct} (psi)
Triaxial Compressive Strength Test	WG/58/4/1					
	WG/58/6/1					
	WG/58/6/2					
	WG/59/78/2					
	WG/59/78/7					
	WG/58/4/1					
	WG/58/4/1					
	WG/58/4/1					
Brazilian Tensile Strength Test	WG/58/1/2					
	WG/58/4/2					
	WG/58/6/3					
	WG/58/8/3					
	WG/58/8/4					
	WG/59/78/3/1					
	WG/59/78/3/2					
	WG/59/78/3/3					
	WG/59/78/3/3					
	WG/59/78/5/2					
	WG/59/78/5/3					

Table A-2. Elastic properties of rock salt samples from Well No. 58 and Well No. 59, Seneca Lake Storage Project, Watkins Glen, New York.

Sample No.	Stage	Elastic Modulus, E ($\times 10^6$ psi)	Poisson Ratio, ν	Shear Modulus, G_1 (\times)	Bulk Modulus, K_1
WG/58/7/2	1				
WG/59/77/3	2				
WG/59/78/1	1				
	2				
Mean \pm Standard Deviation					

Table A-3. Summary of visco-elastic parameters calibrated from the first stages of triaxial creep tests of Syracuse salt from Well no. 58 and no. 59.

Sample No.	σ_1 (psi)	σ_2 (psi)	σ_3 (psi)	τ_{oct} (psi)	σ_{mean} (psi)	η_2 (\times [redacted] psi-day)	G_2 (\times [redacted] psi)	K_2 (\times [redacted] psi)
WG/58/7/1	[redacted]	[redacted]	[redacted]	[redacted]	[redacted]	[redacted]	[redacted]	[redacted]
WG/58/7/3	[redacted]	[redacted]	[redacted]	[redacted]	[redacted]	[redacted]	[redacted]	[redacted]
WG/58/7/2	[redacted]	[redacted]	[redacted]	[redacted]	[redacted]	[redacted]	[redacted]	[redacted]
WG/59/77/2	[redacted]	[redacted]	[redacted]	[redacted]	[redacted]	[redacted]	[redacted]	[redacted]
WG/59/77/3	[redacted]	[redacted]	[redacted]	[redacted]	[redacted]	[redacted]	[redacted]	[redacted]
WG/59/78/1	[redacted]	[redacted]	[redacted]	[redacted]	[redacted]	[redacted]	[redacted]	[redacted]
Mean \pm Standard Deviation						[redacted]	[redacted]	[redacted]

Table A-4. Summary of visco-plastic parameters (η_4) calibrated from the first stages of triaxial creep tests of Syracuse salt from Well no. 58 and no. 59.

Sample No.	σ_1 (psi)	σ_2 (psi)	σ_3 (psi)	τ_{oct} (psi)	σ_{mean} (psi)	η_4 (\times [redacted])
WG/58/7/1	[redacted]	[redacted]	[redacted]	[redacted]	[redacted]	[redacted]
WG/58/7/3	[redacted]	[redacted]	[redacted]	[redacted]	[redacted]	[redacted]
WG/58/7/2	[redacted]	[redacted]	[redacted]	[redacted]	[redacted]	[redacted]
WG/59/77/2	[redacted]	[redacted]	[redacted]	[redacted]	[redacted]	[redacted]
WG/59/77/3	[redacted]	[redacted]	[redacted]	[redacted]	[redacted]	[redacted]
WG/59/78/1	[redacted]	[redacted]	[redacted]	[redacted]	[redacted]	[redacted]
Mean \pm Standard Deviation						[redacted]

APPENDIX B

Results from Finite Element Analysis




Figure B-1. Principal stress distribution in pillar between 34/44 LPG gallery and gallery 10 after both galleries are under hydrostatic pressure of brine for 50 years, obtained from vertical model simulation. The maximum stress in salt is [REDACTED]

[REDACTED]




Figure B-2. Principal stress distribution in pillar between 34/44 LPG gallery and gallery 10 at year 50, obtained from vertical model simulation. The 34/44 LPG gallery is under constant MIT pressure of 1,680 psi (about 80% at casing shoe). The maximum stress in salt is [REDACTED]




Figure B-3. Principal stress distribution in pillar between 34/44 LPG gallery and gallery 10 at year 50, obtained from vertical model simulation. The 34/44 LPG gallery is under constant minimum storage pressure of 1,197 psi (57% at casing shoe). The maximum stress in salt is [REDACTED]




Figure B-4. Principal strain distribution in pillar between 34/44 LPG gallery and gallery 10 after both galleries are under hydrostatic pressure of brine for 50 years, obtained from vertical model simulation. The maximum strain in salt is [REDACTED]




Figure B-5. Principal strain distribution in pillar between 34/44 LPG gallery and gallery 10 at year 50, obtained from vertical model simulation. The 34/44 LPG gallery is under constant MIT pressure of 1,680 psi (about 80% at casing shoe). The maximum strain in salt is 0.8%.




Figure B-6. Principal strain distribution in pillar between 34/44 LPG gallery and gallery 10 at year 50, obtained from vertical model simulation. The 34/44 LPG gallery is under constant minimum storage pressure of 1,197 psi (57% at casing shoe). The maximum strain in salt is [REDACTED]

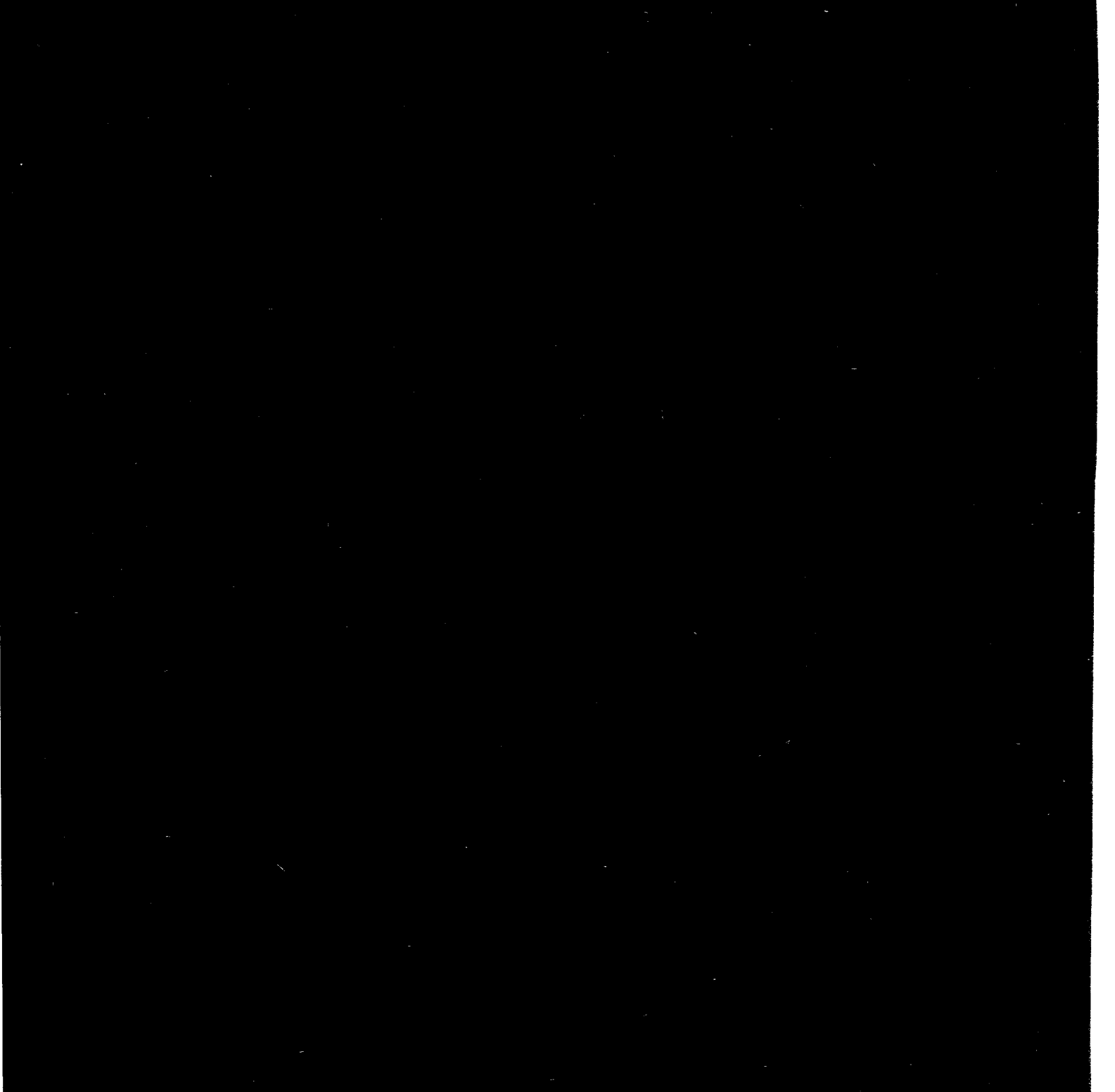


Figure B-7. Principal stress distribution in pillar between 34/44 LPG gallery and gallery 10 after both galleries are under hydrostatic pressure of brine for 50 years, obtained from horizontal model simulation at depth of 2,300 ft. The internal pressure for both galleries is [REDACTED]. The maximum stress in salt is [REDACTED].

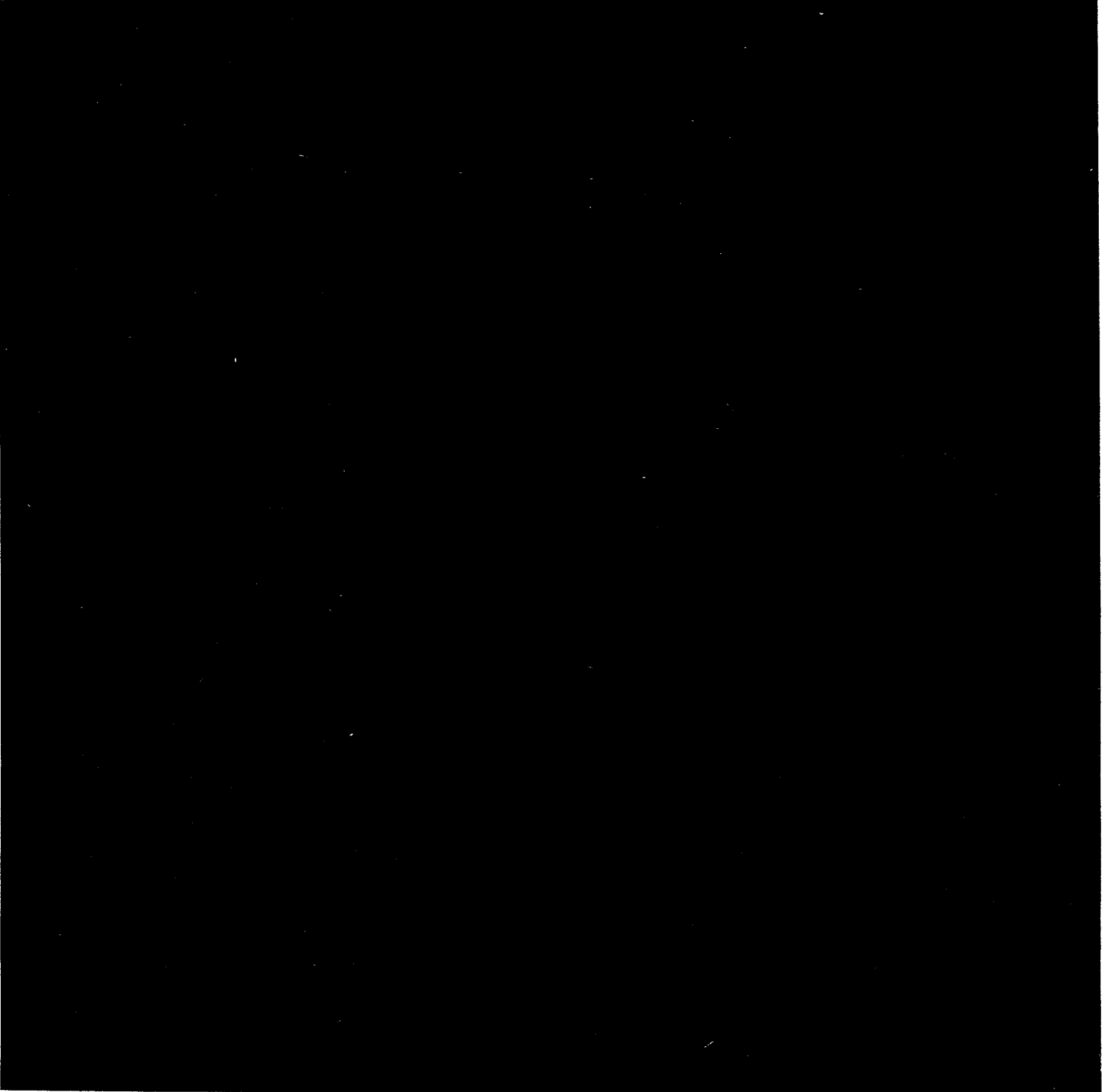


Figure B-8. Principal stress distribution in pillar between 34/44 LPG gallery and gallery 10 at year 50, obtained from horizontal model simulation at depth of 2300 ft. The 34/44 LPG gallery is under constant MIT pressure of 1,784 psi (at 2,300 ft depth). The maximum stress in salt is [REDACTED]




Figure B-9. Principal stress distribution in pillar between 34/44 LPG gallery and gallery 10 at year 50, obtained from horizontal model simulation at 2300 ft depth. The 34/44 LPG gallery is under constant minimum pressure of 1,311 psi. The maximum stress is [REDACTED]

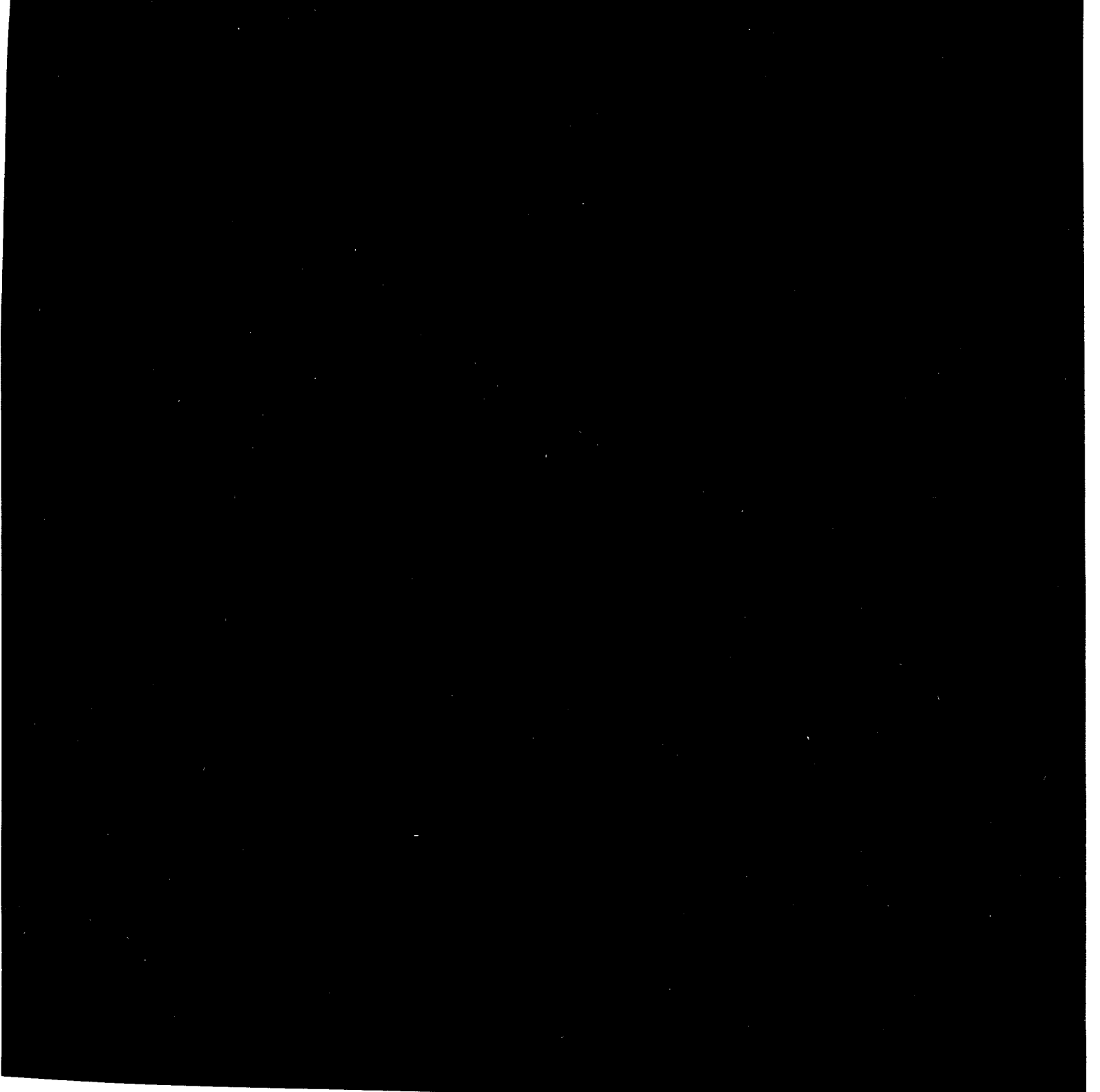


Figure B-10. Principal strain distribution in pillar between 34/44 LPG gallery and gallery 10 after both galleries are under hydrostatic pressure of brine for 50 years, obtained from horizontal model simulation at depth of 2,300 ft. The internal pressure for both galleries is 1,196 psi (at 2,300 ft depth). The maximum strain in salt is [REDACTED]

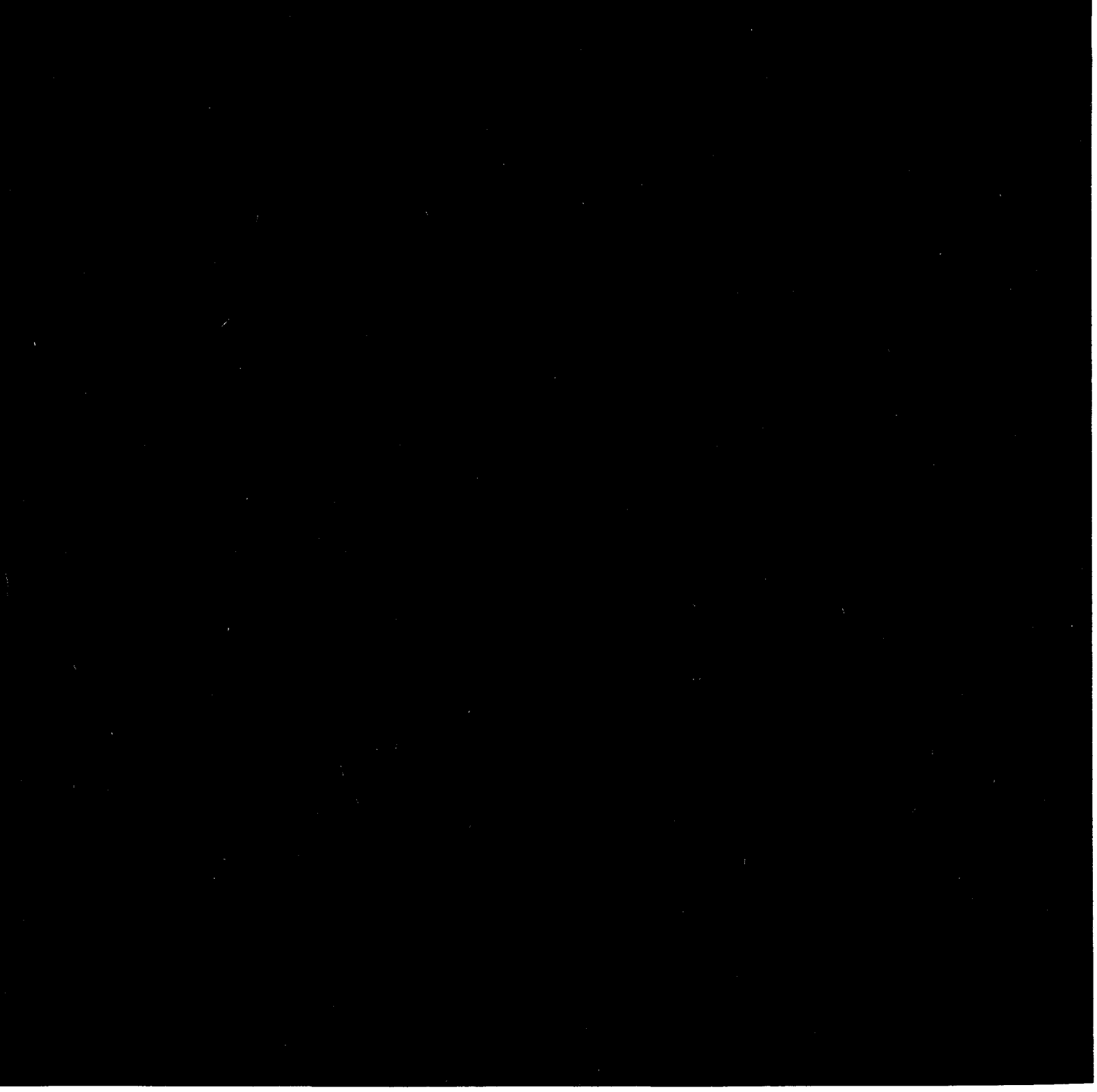


Figure B-11. Principal strain distribution in pillar between 34/44 LPG gallery and gallery 10 at year 50, obtained from horizontal model simulation at depth of 2,300 ft. The 34/44 LPG gallery is under constant MIT pressure of 1,784 psi (at 2,300 ft depth). The maximum strain in salt is [REDACTED]

